Sustainable Energy & Fuels

A Recirculation System for Concentrating CO_2 Electrolyzer Products

Journal:	*Sustainable Energy & Fuels*
Manuscript ID	SE-ART-11-2023-001506.R1
Article Type:	Paper
Date Submitted by the Author:	19-Mar-2024
Complete List of Authors:	Kistler, Tobias; Lawrence Berkeley National Laboratory, Prabhakar, Rajiv Ramanujam; Lawrence Berkeley National Laboratory, Chemical sciences division Agbo, Peter; Lawrence Berkeley National Laboratory, Chemical Sciences

A Recirculation System for Concentrating CO_2 Electrolyzer Products

Tobias A. Kistler[1,2], Rajiv R. Prabhakar[1,2], Peter Agbo[1,2,*]

[1]Chemical Sciences Division, Lawrence Berkeley National Laboratory, Berkeley, California 94720, USA

[2]Liquid Sunlight Alliance, Lawrence Berkeley National Laboratory, Berkeley, California 94720, USA

[*]Corresponding Author: pagbo@lbl.gov

Abstract

Electrochemical carbon dioxide reduction represents a promising path to utilize CO_2 as a feedstock for generating valuable products such as fuels and chemicals. Faradaic efficiencies near 100% have been achieved for certain CO_2 reduction products such as CO, but the electrolyzer outlet streams usually contain large fractions of unreacted CO_2, dropping the product concentrations below 1% in many cases. The system disclosed here recycles the unreacted CO_2 together with the products and flows them back into the CO_2 reduction reactor, enabling much higher CO_2 conversion rates without dropping the gas flow rate. However, simple recirculation is shown to accumulate significant amounts of hydrogen, impeding effective CO_2 reduction. In this looped system, an electrochemical H_2 pump is placed in series with the CO_2 reactor, which effectively removes all the H_2 from the recycled gas stream, increasing the concentrations of carbon-containing products. The system was initially tested with a CO-generating catalyst and CO concentrations above 70% were achieved in the recycled gas stream, compared to a maximum CO concentration of 8% in single-pass configuration. Results with a CO_2 reactor targeting ethylene as the main product show that ethylene concentrations of at least 10% can be achieved, which is roughly 20 times higher compared to a single-pass system.

Introduction

Ethylene is the largest-volume synthetic organic chemical world-wide, predominantly produced from steam cracking of alkanes.[1–4] This traditional process of making ethylene generates the greenhouse gas carbon dioxide in significant quantities as a byproduct. In an age of rising temperatures due to increasing CO_2 concentrations in the atmosphere, an alternative, more environmentally friendly process becomes highly desirable. Electrochemical CO_2 reduction is a particularly promising path since it uses CO_2 as a feedstock – rather than generating it as a byproduct – to produce ethylene.

Since the initial reports of Hori *et al.*,[5,6] much progress has been made towards improving the efficiency of electrochemical CO_2 reduction to ethylene, particularly by tuning the microenvironment of Cu catalysts.[7–12] However, most publications in the recent literature report ethylene concentrations below 10% in electrolyzer outlet streams, even with faradaic efficiencies above 50% and current densities higher than 1 A cm^{-2}. In many of these reports, ethylene is actually produced at concentrations well below 1% (**Fig. 1** and **Table S1**).[13–26]

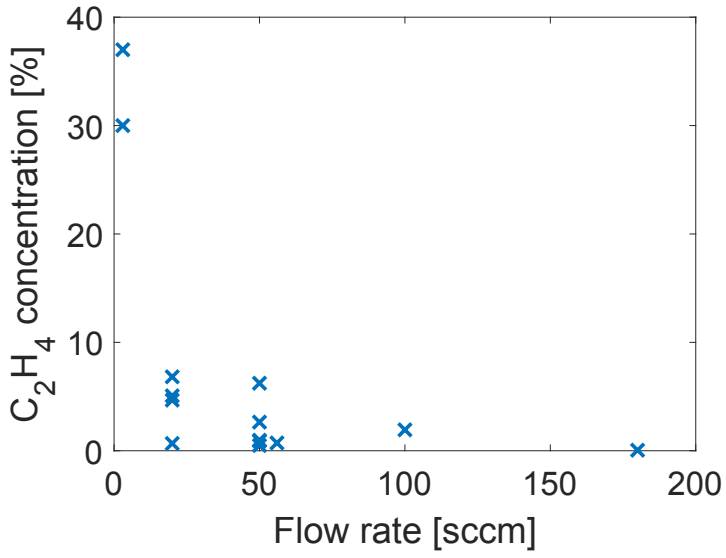

Fig. 1 Ethylene concentration values as a function of the cathode gas flow rate, calculated from recent reports in the literature.[13–26] Detailed values are shown in **Table S1** together with the calculation method.

To date, ethylene concentrations above 10% have only been achieved by reducing the inlet flow rate of CO_2 significantly. However, this can lead to problematic flow conditions that starve catalytic sites of CO_2, quickly resulting in the hydrogen evolution reaction (HER) dominating over CO_2 reduction, and reducing CO_2 electrolyzer performance. Additionally, current literature would suggest, as embodied in **Fig. 1**, that it is not clear if ethylene concentrations above 40% could ever be reached by further reducing the CO_2 flow rates.

An alternative way to increase C_2H_4 concentrations in the outlet stream and simultaneously enhance CO_2 utilization is to recirculate the generated fuel stream back into the electrolyzer. However, using a recirculation system will also concentrate any byproducts from CO_2-to-C_2H_4 conversion, such as H_2, which we show can impede the production of ethylene. Therefore, we decided to develop a looped system for CO_2 reduction that employs a hydrogen pump to remove H_2 from the gas loop. While the operation of an H_2 pump is generally challenging under conditions of high carbon monoxide concentrations, which effectively poisons the employed Pt catalysts, moving to temperatures above 160 °C can circumvent these poisoning issues, provided appropriate materials are chosen.[27] With the above-mentioned recycling system, we were able to produce a gas stream with a peak ethylene concentration of 9.4%, a value roughly 20 times higher than that achieved using a single-pass system operated under comparable conditions.

Materials and methods

System architecture

A simplified version of the CO_2 gas recycling setup is displayed in **Fig. 2** and the detailed diagram is shown in **Fig. S1**.

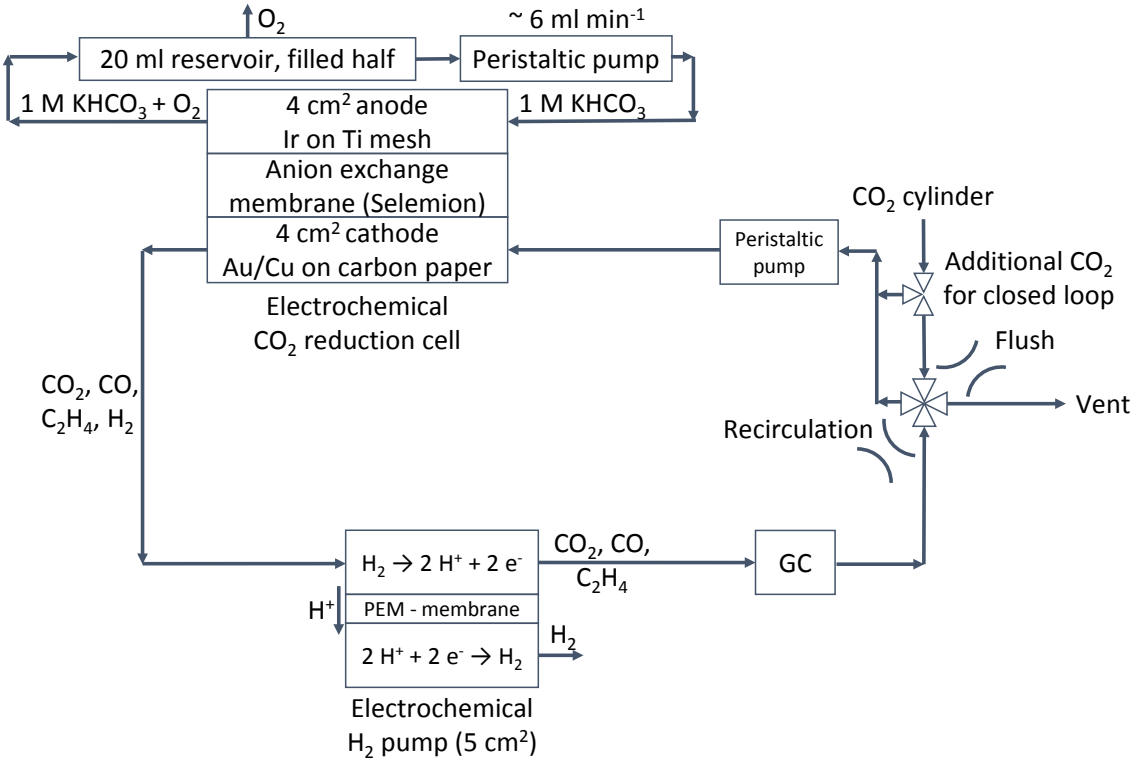

Fig. 2 CO_2 gas recirculation system consisting of a 4 cm^2 electrochemical CO_2 reduction cell, a 5 cm^2 electrochemical H_2 pump with proton-exchange membrane (PEM), a gas chromatograph (GC), a 4-way valve to open/close the gas loop, a 3-way valve to enable flow of fresh CO_2 into the loop and a peristaltic pump to move the gases. A more detailed diagram of the setup can be seen in **Fig. S1**.

Initially, CO_2 flows from the gas cylinder through a peristaltic pump and then through the cathode of a CO_2 reduction cell, the anode of a hydrogen pump and a gas chromatograph until it reaches a 4-way valve where the mixed gas stream is vented. The CO_2 reduction cell was tested with Au and Cu catalysts in the cathode chamber, and generally produced a gas mix of H_2, CO and C_2H_4 (no C_2H_4 with Au). The gas mix from the CO_2 reduction cell outlet then flows into the H_2 pump where H_2 is selectively oxidized, yielding a pure stream of H_2 and a gas mix in the loop which is essentially free of H_2. After air is flushed from the system and the system

yields a stable performance, the 4-way valve is turned into recirculation mode, guiding the gas mix from the CO_2 reduction cell outlet back to its inlet. An additional 3-way valve was installed to enable the addition of fresh CO_2 into the closed gas loop, as a way of regulating CO_2 partial pressure in the system.

CO_2 reduction cell materials

A 4 cm^2 platinized Ti mesh (~270 µm thick) was coated with 100 nm of Ir (0.23 mg cm^{-2}) by sputtering and used as the anode of the cell. For the cathode, 4 cm^2 large carbon paper (AvCarb GDS2230, 275 µm thick) with a hydrophobic, micro-porous layer (MPL) was sputtered with either 100 nm of Cu (0.09 mg cm^{-2}) or 100 nm of Au (0.19 mg cm^{-2}). Selemion AMV membranes (chloride form, ~100 µm thick) from AGC Engineering were used to separate anode and cathode. The endplates were machined from polymethylmethacrylate containing straight flow channels for the anode and serpentine flow channels for the cathode compartment. Laser-cut, window frame-shaped silicone pieces served as gaskets. The thickness of the gaskets and the torque of the screws (0.1 N m) determined the cell compression. The electrodes were contacted by 25 µm thick tantalum strips, which were connected to the potentiostat clamps.

H_2 pump materials

An acid-compatible 5 cm^2 cell from Fuel Cell Technologies Inc. with aluminum endplates, gold-coated current collectors and graphite/Ti flowfields with serpentine flow channels for the anode/cathode was used as the hydrogen pump. Celtec P1100W Anode material (Fuel Cell Store), consisting of a woven carbon cloth with MPL and a Pt catalyst with a loading of ~1 mg cm^{-2}, was used for both the anode and cathode, which were separated by a high-temperature Celtec-P membrane (Fuel Cell Store). Teflon gaskets were employed to achieve roughly 20% compression of the electrodes by tightening the cell bolts to 4.5 N m.

Measurement conditions

Unless otherwise mentioned, the following experimental conditions were used. A peristaltic pump pushed 1M $KHCO_3$ at a flow rate of ~6 mL min^{-1} through the anode chamber of the CO_2 reduction cell. $KHCO_3$ electrolytes were prepared using ACS reagent-grade powder from Sigma-Aldrich. CO_2 was recirculated using a peristaltic pump and the pump tubing's inner diameter was varied to change the flow rate. The pressure in the gas loop was controlled with a pressure regulator and by adjusting the flow rate of fresh CO_2 entering the loop. A mass flow meter was used to precisely measure the flow rate and pressure in the gas loop. Argon was flowed at 5 sccm to flush the cathode of the hydrogen pump and aid with accurate product detection via gas chromatography. During the heating phase of the H_2 pump, argon was also flowing through the anode side. After the temperature equilibrated, the anode gas flow was changed to H_2 or the outlet of the CO_2 reduction cell. All electrochemical measurements were performed in 2-electrode configuration and cyclic voltammograms were measured with a scan rate of 10 mV s^{-1}.

Product analysis

The recycled gas stream was fed into a gas chromatograph in the gas loop from SRI Instruments (Multiple Gas Analyzer #5, 8610C) equipped with a thermal conductivity detector and flame ionization detector (FID). Prior to the FID, all products went through a methanizer to increase the minimum detection limit of some carbon-based products. The highest CO concentration available for calibration of the FID was 8.12%. If CO concentrations exceeded the calibration limits, a calibration curve for CO_2, which was established for concentrations up to 100%, was used for calculating CO concentrations. Since both CO and CO_2 are methanized before detection with the FID, they can be expected to yield very similar calibration curves. Liquid products were quantified using Nuclear Magnetic Resonance (500 MHz Bruker) with 0.05M

phenol and 0.01M dimethyl sulfoxide as the internal standards for quantification. A pre-saturation sequence was used to suppress the water peak. Quantification was done with 400 μL of anolyte used for CO_2 reduction and then added to 50 μL of internal standard solution and 50 μL of D_2O. The detailed determination of product concentrations is described by Prabhakar *et al*.[28,29] It should be noted that liquid products were only detected in the anode, where product re-oxidation is possible and may potentially skew faradaic efficiencies.

X-ray photoelectron spectroscopy (XPS)

The chemical composition of Cu and Au electrocatalysts (Cu 2p and Au 4f) was obtained by XPS on a Kratos Axis Ultra DLD system at a take-off angle of 0° relative to the surface normal. An Al Kα source (hν = 1,486.6 eV) was used with a pass energy of 20 eV for the narrow scan of core levels and valence band spectra with a step size of 0.05 eV and 0.025 eV, respectively.

Results and discussion

Hydrogen pump characterization

Before integration into the gas recycling loop, the hydrogen pump was characterized separately. Since hydrogen oxidation reaction (HOR) is catalyzed by the anode of the H_2 pump and HER occurs at the cathode, the thermodynamic voltage for these coupled cell reactions is 0 V. Under feed conditions of pure H_2, the maximum current can be determined as a function of the anode flow rate (I_{max} = 131 mA $sccm^{-1}$) assuming a faradaic efficiency for HOR of 100%. As shown in **Fig. 3**a, the maximum current is achieved at voltages as low as 0.1-0.2 V, indicating low overpotentials.

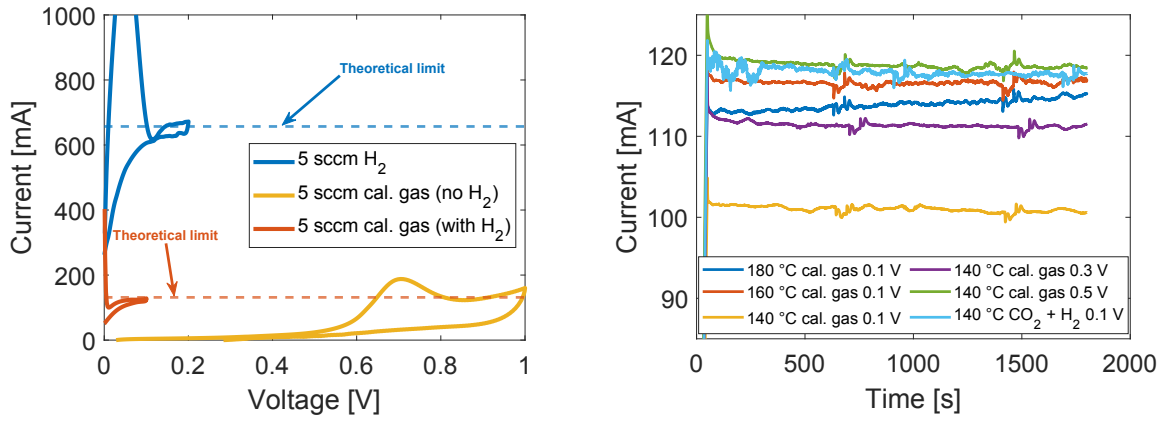

(a) (b)

Fig. 3 Performance testing of the hydrogen pump with different anode feed gas compositions. (a) Cyclic voltammetry measurements at 180 °C indicate that the H_2 pump operates near the theoretical limit even when fed by a CO-containing calibration gas (15.9% H_2, 2.6% CO, 1.7% CH_4, 0.9% C_2H_4, 0.7% C_2H_6, 78.3% CO_2). (b) Short-term stability tests with calibration gas (16.7% H_2, 6.8% CO, 4.2% CH_4, 3.3% C_2H_4, 2.5% C_2H_6, 66.5% CO_2) and CO-free feed (15.5% H_2, 84.5% CO_2), flowing at 5 sccm at different cell temperatures and voltages, indicate CO poisoning effects at temperatures below 160 °C. The small current fluctuations appearing roughly every 800 s are caused by slight pressure changes due to GC injections.

The initial current spike around 0.1 V in the forward scan direction can be explained by accumulation of H_2 near the H_2 pump's anode, temporarily enabling the current to go beyond the theoretical limit at the beginning of the measurement. Since Pt catalysts were used to support HOR and HER, it is important to consider CO poisoning effects, as CO binds tightly to Pt at room temperature. However, sufficiently high temperatures can prevent CO accumulation on the Pt surface, enabling long-term operation.[27] To investigate these effects, the H_2 pump was fed with a calibration gas containing both H_2 and CO (**Fig. 3**a). In this case, the theoretical current limit was again achieved at low voltages near 0.1 V, indicating that CO poisoning is absent when the cell is heated to 180 °C. Furthermore, HOR is not the only possible reaction at the anode of the H_2 pump. For example, CO or ethylene oxidation to CO_2 can also be coupled

to HER at the cathode. For this reason, a hydrogen-free calibration gas was fed to the H_2 pump's anode and the current measured as a function of the applied bias (**Fig. 3**a). During this test, no current is observed until ~0.5 V, at which point the overpotential is sufficiently high to drive oxidation of carbon-based molecules. Therefore, to prevent re-oxidation of CO_2 reduction products in the gas recycling loop displayed in **Fig. 2**, it is important to operate the H_2 pump at voltages below 0.5 V.

In a second series of tests, the minimum H_2 pump temperature to prevent CO poisoning was examined (**Fig. 3**b). Lower temperatures are desirable for reducing operating costs and if side reactions such as ethylene hydrogenation to ethane are to be minimized, which may occur on the hot anode surface if ethylene and H_2 concentrations are sufficiently high and the cell is not biased. The cell was again heated to 180 °C and tested, followed by temperatures of 160 °C and 140 °C. While the performance between 160 °C and 180 °C is very similar at 0.1 V, the current drops significantly at 140 °C and hydrogen was detected at the anode outlet (**Fig. S2**), indicating that not all of the H_2 was pumped across the membrane. While switching to higher applied voltages of 0.3 and 0.5 V can recover some of the current (**Fig. 3**b) and pump more H_2 across the membrane (**Fig. S2**), it increases the risk of carbon-based molecules oxidation in the anode and is therefore not desirable. To confirm that CO is the performance-limiting factor at 140 °C, the H_2 pump was also tested with a gas containing only H_2 and CO_2, which shows similar performance to the tests at higher temperatures with no signs of CO poisoning (**Fig. 3**b). In summary, it can be concluded that the minimum operating temperature to prevent CO poisoning is 160 °C.

CO_2 reduction to CO

After the performance of the H_2 pump was characterized, the gas recycling system shown in **Fig. 2** was assembled and tested using a Au catalyst on the cathode of the CO_2 reduction cell.

In this configuration the main expected products from CO_2 reduction are H_2 and CO. Since H_2 is removed from the recycled gas stream by the H_2 pump, CO is expected to accumulate over time in the closed loop. An initial test with this system yielded a CO concentration of ~40% after 6 h of operation, up from 2% when using only single-pass conversion (**Fig. S3**). While this level of product accumulation marks a significant improvement, this experiment also revealed that a large fraction of gas concentrations could not be accounted for. Besides H_2, CO and CO_2, the only other gas expected in the looped stream is the carrier gas from the GC. Since the recycled gas stream flows directly through the sample loop of the GC, every injection of the GC will push carrier gas into the closed loop when the GC valve switches back to the default position. The concentration of the carrier gas in the loop cannot be measured directly by the GC but can be estimated by the volume of the sample loop (**Fig. S4**a). However, a control experiment with only CO_2 recirculating in the loop revealed that the concentration of carrier gas in the loop can be much larger than expected since the carrier gas in the GC is pressurized, leading to a ~3x higher concentration than initially estimated (**Fig. S4**b). Therefore, the standard valve setup of the GC was modified to prevent carrier gas from entering the gas loop (**Fig. S5**).

Another experiment was carried out with the modified GC valve setup, again targeting CO as the main product with the gas recycling system. Since carrier gas is now absent in the recycled gas stream, the CO concentration reached a much higher peak value of 72.5% (**Fig. 4**a), nearly doubling the concentration compared to the test without the modified GC valve setup (**Fig. S3**).

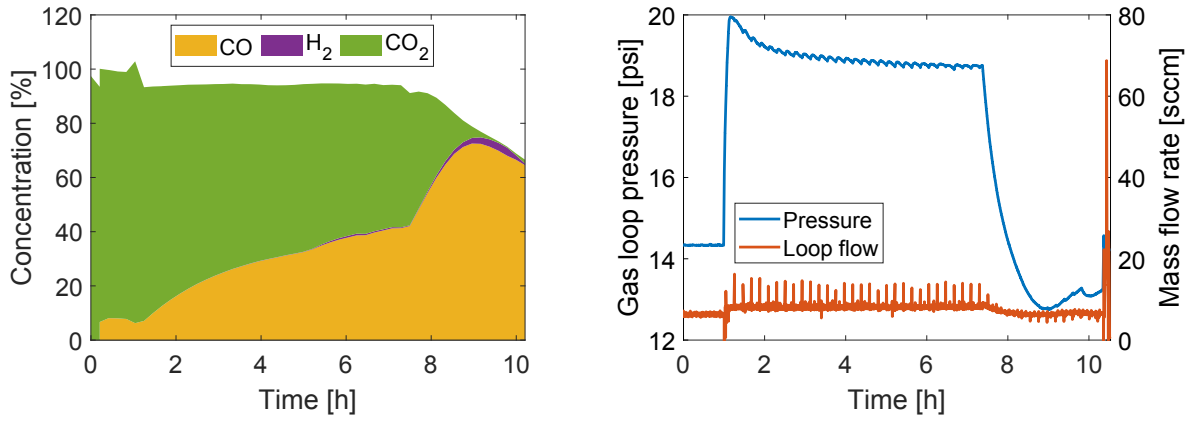

(a) (b)

Fig. 4 Recirculation experiment performed with Au as the CO_2 reduction catalyst, operated at 3 V. (a) Concentration of gases in the recycling loop (in mol %). After 1 h of operation, the loop was closed and after 7.5 h, the flow of fresh CO_2 was stopped. (b) Pressure and mass flow rate in the recycling loop.

During the first hour of the experiment, the CO concentration equilibrated near 8% using only single-pass conversion, after which the gas loop was closed, explaining the rise in CO concentration over time. After the loop was closed, the pressure in the gas stream was controlled via the flow rate of fresh CO_2 flowing into the loop and set to ~19 psi (**Fig. 4**b). After 6.5 h of operation in closed loop mode, the addition of CO_2 was stopped, causing a rapid pressure decrease since the remaining CO_2 in the loop is consumed via reaction to CO and carbonate crossover through the membrane, and produced hydrogen is removed through the H_2 pump. After CO_2 was removed from the loop, a peak CO concentration of 72.5% was achieved at minimal concentrations of H_2.

In this case, the missing gas concentrations may be explained by a gas leak of the system, which allowed air to enter the loop as the loop pressure dropped below ambient pressure (~14.4 psi). Control experiments showed that the leak is not coming from any of the electrochemical cells, but likely arises from the tubing installed in the peristaltic pump. Other pumps which are

specifically designed to be leak-free for gases, such as gas-tight diaphragm pumps, are expected to yield even higher peak CO concentrations. Alternatively, the tubing around the pump could be put into a CO_2 atmosphere, also preventing any air from entering the gas loop. However, this was beyond the scope of this manuscript. As shown by XPS measurements taken before and after this looped experiment, the Au catalyst composition was stable (**Fig. S6**).

CO_2 reduction to Ethylene

In a separate set of experiments, the potential of the gas recycling loop to concentrate ethylene was examined. For this reason, the Au catalyst on the CO_2 reduction cell's cathode was swapped to a Cu catalyst. Initial tests in single-pass configuration indicate that C_2H_4 concentrations below 0.5% can be expected for gas flow rates of 7 sccm or higher (**Fig. S7**).

Switching from single-pass configuration to gas stream recirculation yielded C_2H_4 concentrations near 1% if no H_2 pump is used (**Fig. S8**). This recycling experiment clearly demonstrated that H_2 accumulates very quickly with an exponential trend in the absence of an H_2 pump, prohibiting the accumulation of C_2H_4. The exponential trend of HER can be explained by the decreasing availability of CO_2 as HER starts to dominate, reducing the chances of CO_2 reduction and further enhancing the rate of HER, resulting in a self-accelerating switch to HER.

Similarly, a separate single-pass experiment was carried out where the CO_2 cathode inlet feed was diluted step-by-step with inert Ar gas (**Fig. S9**). As the concentration of CO_2 was reduced, the total device current increased quickly due to rising HER, with lower concentrations of CO_2 leading to a sharper increase of HER. This test also indicated that higher inlet flow rates enable operation with lower feed concentrations of CO_2 without leading to dominating HER.

As a next step, the hydrogen pump was integrated into the gas recycling loop as displayed in **Fig. 2**, and the whole system was operated. The result was a peak C_2H_4 concentration of 4.8% (**Fig. S10**), a value roughly 5x larger than that without integration of the H_2 pump. However, within one hour of operation in closed loop mode, all of the CO_2 in the gas loop was reacted or lost to carbonate crossover through the anion exchange membrane of the CO_2 reduction cell, preventing further product accumulation.

After the test shown in **Fig. S10**, the gas loop was opened and all the accumulated products were flushed out for one hour. Afterwards, the gas loop was closed again at 3 h total operation time with fresh CO_2 constantly flowing into the closed gas loop during this experiment. This enabled longer operation times and higher C_2H_4 concentrations, while keeping the pressure in the loop near atmospheric pressure (**Fig. 5**).

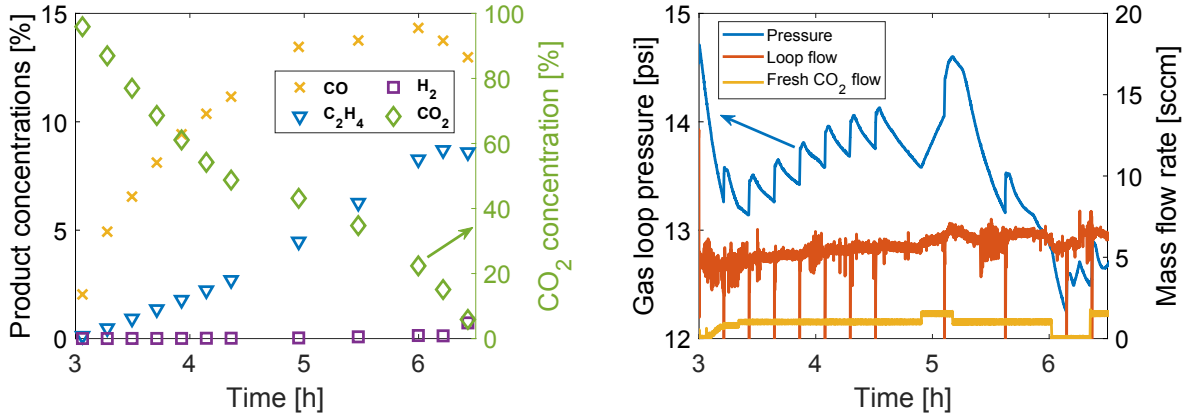

(a) (b)

Fig. 5 Recirculation experiment performed with Cu as the CO_2 reduction catalyst, operated at 4 V. The same system as in **Fig. S10** was used and the gas loop was closed again after 3 h for this run. (a) Product and CO_2 concentrations over time, indicating a peak C_2H_4 concentration of 8.7% after 3 h of closed loop operation (6 h total operation time). (b) Pressure and mass flow rate in the gas loop. The mass flow rate of fresh CO_2 was tuned to stabilize the loop pressure. Pressure spikes are due to GC injections.

Due to the longer operation time of the closed loop system, an ethylene concentration of 8.7% was achieved. Interestingly, the concentration of CO also increased over time even though CO is a known intermediate for C_2H_4 generation,[30] suggesting that produced CO is not likely to react further after its desorption. Modification of the catalytic microenvironment in the CO_2 electrolyzer cathode may enhance re-adsorption of CO and its subsequent conversion to C_2H_4, representing a promising pathway to even higher C_2H_4 concentrations.

While for the CO_2 reduction to CO system (**Fig. 4**), it was beneficial to operate slightly above ambient pressure to prevent air from entering the gas loop, elevated gas pressure is expected to drop the faradaic efficiency for C_2H_4 on Cu catalysts and promote formate generation.[31] For this reason, the pressure was kept near ambient pressure with the Cu-based system, enabling air to enter the gas loop more easily and dilute the formed products while adding the possibility of oxygen reduction reaction as another possible, undesirable side reaction in the CO_2 reduction cell. XPS measurements taken before and after this looped experiment indicate a change in the Cu catalyst composition. Specifically, the relative intensities of the Cu (0/I) and Cu (II) 2p core levels are shown to switch during operation, with Cu (II) signals becoming more prominent after CO_2R operation (**Fig. S11**).

The effect of the gas leak in the loop becomes even more evident during a longer, 24-hour closed loop experiment (**Fig. S12**). After 10 h of operation, increases in ethylene and CO concentration were arrested, indicating that formation of CO_2 reduction products equaled their leak rate, resulting in dropping faradaic efficiencies over time. After the flow of fresh CO_2 was stopped in this longer test, a peak C_2H_4 concentration of 9.4% was reached, only a marginal improvement over the 3-hour test shown in **Fig. 5** considering the much longer operation time. However, this peak value marks a roughly 20-fold improvement over the single-pass system

operated at a similar flow rate (**Fig. S7**). Furthermore, a propylene concentration near 0.5% was also detected during this experiment (**Fig. S12**d).

Finally, the peak concentration achieved with the CO_2 reduction cell within the described closed loop system was compared to the same CO_2 reduction cell operated in single-pass configuration at the minimum gas flow rate that maximizes ethylene outlet concentrations. At a much-reduced outlet flow rate of ~0.8 sccm, the CO_2 reduction cell yielded an C_2H_4 concentration of 7.5% (**Fig. S13**), a value which is lower than with the gas recirculation system even with the present gas leaks. In fact, if inert gases in the closed loop system are ignored (no leaks), the peak C_2H_4 concentration is actually 37.9%, which is 5 times higher than what is possible with the single-pass system operating at a significantly reduced flow rate.

Conclusion

Ethylene production at significant concentrations is necessary to make CO_2 reduction viable for commercial applications and enable its steady-state coupling to downstream chemistries such as ethylene oligomerization. We demonstrated successful operation of a gas recycling system which accumulates CO_2 reduction products by incorporating a hydrogen pump that produces a pure stream of H_2 as a byproduct. CO concentrations of at least 72.5% (96.9% ignoring leaks) were demonstrated using a Au catalyst. Swapping to a Cu catalyst with faradaic efficiencies of ~20% for C_2H_4 yielded C_2H_4 concentrations of at least 9.4% (37.9% ignoring leaks). This marks a 20-fold increase in C_2H_4 concentration compared to a single-pass system operated at a similar flow rate and also shows a path for going beyond the limits associated with ultra-low flow single-pass systems. Finally, while the demonstrated values mark a significant improvement over single-pass systems, it can reasonably be expected that even higher C_2H_4

concentrations are achievable with a more selective CO_2 reduction cell that produces C_2H_4 at faradaic efficiencies over 50% or is more efficient at reducing any produced CO to C_2H_4.

Acknowledgements

The authors thank Xiong Peng for his helpful insights. This material is based on work performed by the Liquid Sunlight Alliance, which is supported by the U.S. Department of Energy, Office of Science, Office of Basic Energy Sciences, Fuels from Sunlight Hub under Award Number DE-SC0021266.

Conflict of Interest

The authors declare the following competing financial interest(s): The contents of this paper relate to a 2023 patent application by Lawrence Berkeley National Laboratory, with T.K. and P.A. listed as inventors.

References

1 P. E. Haynes and G. O. Curme, Jr, US Pat., US1460545A, 1923.
2 C. W. Fernelius, H. Wittcoff and R. E. Varnerin, *J. Chem. Educ.*, 1979, **56**, 385.
3 R. van Mao, H. Yan, A. Muntasar and N. Al-Yassir, in *New and Future Developments in Catalysis*, ed. S. L. Suib, Elsevier, 2013, pp. 143–173.
4 A. S. Bin Naqyah and A. A. Al-Rabiah, *ACS Omega*, 2022, **7**, 28445–28458.
5 Y. Hori, K. Kikuchi, A. Murata and S. Suzuki, *Chem. Lett.*, 1986, **15**, 897–898.
6 Y. Hori, A. Murata, R. Takahashi and S. Suzuki, *J. Am. Chem. Soc.*, 1987, **109**, 5022–5023.
7 J. Qu, X. Cao, L. Gao, J. Li, L. Li, Y. Xie, Y. Zhao, J. Zhang, M. Wu and H. Liu, *Nano-Micro Lett.*, 2023, **15**, 178.
8 B. Zhang, J. Zhang, M. Hua, Q. Wan, Z. Su, X. Tan, L. Liu, F. Zhang, G. Chen, D. Tan, X. Cheng, B. Han, L. Zheng and G. Mo, *J. Am. Chem. Soc.*, 2020, **142**, 13606–13613.
9 M. G. Kibria, C.-T. Dinh, A. Seifitokaldani, P. de Luna, T. Burdyny, R. Quintero-Bermudez, M. B. Ross, O. S. Bushuyev, F. P. García de Arquer, P. Yang, D. Sinton and E. H. Sargent, *Adv. Mater.*, 2018, **30**, e1804867.
10 C. Choi, S. Kwon, T. Cheng, M. Xu, P. Tieu, C. Lee, J. Cai, H. M. Lee, X. Pan, X. Duan, W. A. Goddard and Y. Huang, *Nat. Catal.*, 2020, **3**, 804–812.
11 Y. Chen, Z. Fan, J. Wang, C. Ling, W. Niu, Z. Huang, G. Liu, B. Chen, Z. Lai, X. Liu, B. Li, Y. Zong, L. Gu, J. Wang, X. Wang and H. Zhang, *J. Am. Chem. Soc.*, 2020, **142**, 12760–12766.

12 C.-T. Dinh, T. Burdyny, M. G. Kibria, A. Seifitokaldani, C. M. Gabardo, F. P. García de Arquer, A. Kiani, J. P. Edwards, P. de Luna, O. S. Bushuyev, C. Zou, R. Quintero-Bermudez, Y. Pang, D. Sinton and E. H. Sargent, *Science (New York, N.Y.)*, 2018, **360**, 783–787.

13 C. M. Gabardo, C. P. O'Brien, J. P. Edwards, C. McCallum, Y. Xu, C.-T. Dinh, J. Li, E. H. Sargent and D. Sinton, *Joule*, 2019, **3**, 2777–2791.

14 W. H. Lee, C. Lim, S. Y. Lee, K. H. Chae, C. H. Choi, U. Lee, B. K. Min, Y. J. Hwang and H.-S. Oh, *Nano Energy*, 2021, **84**, 105859.

15 F. Li, A. Thevenon, A. Rosas-Hernández, Z. Wang, Y. Li, C. M. Gabardo, A. Ozden, C. T. Dinh, J. Li, Y. Wang, J. P. Edwards, Y. Xu, C. McCallum, L. Tao, Z.-Q. Liang, M. Luo, X. Wang, H. Li, C. P. O'Brien, C.-S. Tan, D.-H. Nam, R. Quintero-Bermudez, T.-T. Zhuang, Y. C. Li, Z. Han, R. D. Britt, D. Sinton, T. Agapie, J. C. Peters and E. H. Sargent, *Nature*, 2020, **577**, 509–513.

16 J. Li, A. Ozden, M. Wan, Y. Hu, F. Li, Y. Wang, R. R. Zamani, D. Ren, Z. Wang, Y. Xu, D.-H. Nam, J. Wicks, B. Chen, X. Wang, M. Luo, M. Graetzel, F. Che, E. H. Sargent and D. Sinton, *Nat. Commun.*, 2021, **12**, 2808.

17 Y.-R. Lin, D. U. Lee, S. Tan, D. M. Koshy, T. Y. Lin, L. Wang, D. Corral, J. E. Avilés Acosta, J. A. Zamora Zeledon, V. A. Beck, S. E. Baker, E. B. Duoss, C. Hahn and T. F. Jaramillo, *Adv. Funct. Mater.*, 2022, **32**, DOI: 10.1002/adfm.202113252.

18 W. Liu, P. Zhai, A. Li, B. Wei, K. Si, Y. Wei, X. Wang, G. Zhu, Q. Chen, X. Gu, R. Zhang, W. Zhou and Y. Gong, *Nat. Commun.*, 2022, **13**, 1877.

19 W. Ma, S. Xie, T. Liu, Q. Fan, J. Ye, F. Sun, Z. Jiang, Q. Zhang, J. Cheng and Y. Wang, *Nat. Catal.*, 2020, **3**, 478–487.

20 I. Merino-Garcia, J. Albo, J. Solla-Gullón, V. Montiel and A. Irabien, *J. CO2 Util.*, 2019, **31**, 135–142.

21 D.-H. Nam, O. Shekhah, A. Ozden, C. McCallum, F. Li, X. Wang, Y. Lum, T. Lee, J. Li, J. Wicks, A. Johnston, D. Sinton, M. Eddaoudi and E. H. Sargent, *Adv. Mater.*, 2022, **34**, e2207088.

22 A. Ozden, F. Li, F. P. García de Arquer, A. Rosas-Hernández, A. Thevenon, Y. Wang, S.-F. Hung, X. Wang, B. Chen, J. Li, J. Wicks, M. Luo, Z. Wang, T. Agapie, J. C. Peters, E. H. Sargent and D. Sinton, *ACS Energy Lett.*, 2020, **5**, 2811–2818.

23 R. Wang, J. Liu, Q. Huang, L.-Z. Dong, S.-L. Li and Y.-Q. Lan, *Angew. Chem., Int. Ed. Engl.*, 2021, **60**, 19829–19835.

24 Y. N. Xu, W. Li, H. Q. Fu, X. Y. Zhang, J. Y. Zhao, X. Wu, H. Y. Yuan, M. Zhu, S. Dai, P. F. Liu and H. G. Yang, *Angew. Chem.*, 2023, **135**, DOI: 10.1002/ange.202217296.

25 Z. Wang, Y. Li, X. Zhao, S. Chen, Q. Nian, X. Luo, J. Fan, D. Ruan, B.-Q. Xiong and X. Ren, *J. Am. Chem. Soc.*, 2023, **145**, 6339–6348.

26 M. Zhong, K. Tran, Y. Min, C. Wang, Z. Wang, C.-T. Dinh, P. de Luna, Z. Yu, A. S. Rasouli, P. Brodersen, S. Sun, O. Voznyy, C.-S. Tan, M. Askerka, F. Che, M. Liu, A. Seifitokaldani, Y. Pang, S.-C. Lo, A. Ip, Z. Ulissi and E. H. Sargent, *Nature*, 2020, **581**, 178–183.

27 G. Venugopalan, D. Bhattacharya, E. Andrews, L. Briceno-Mena, J. Romagnoli, J. Flake and C. G. Arges, *ACS Energy Lett.*, 2022, **7**, 1322–1329.

28 R. R. Prabhakar, R. Lemerle, M. Barecka, M. Kim, S. Seo, E. N. Dayi, I. Dei Tos and J. W. Ager, *J. Mater. Chem. A*, 2023, **11**, 13588–13599.

29 T. Chatterjee, E. Boutin and M. Robert, *Dalton Trans.*, 2020, **49**, 4257–4265.

30 S. Nitopi, E. Bertheussen, S. B. Scott, X. Liu, A. K. Engstfeld, S. Horch, B. Seger, I. E. L. Stephens, K. Chan, C. Hahn, J. K. Nørskov, T. F. Jaramillo and I. Chorkendorff, *Chem. Rev.*, 2019, **119**, 7610–7672.

31 L. Huang, G. Gao, C. Yang, X.-Y. Li, R. K. Miao, Y. Xue, K. Xie, P. Ou, C. T. Yavuz, Y. Han, G. Magnotti, D. Sinton, E. H. Sargent and X. Lu, *Nat. Commun.*, 2023, **14**, 2958.